Enhanced electro active properties of NiCo2O4 nanostructures using garlic extract for the sensitive and selective enzyme-free detection of ascorbic acid

Abdul Ghaffar Solangi, Aneela Tahira, Abdul Sattar Chang, Tajnees Pirzada, Zulfiquar Ali Solangi, Fouzia Chang, Muhammad Ali Bhatti, Adeel Liaquat Bhatti, Shusheel Kumar, Abdul Hanan, et al.

Enhanced electro active properties of $NiCo_2O_4$ nanostructures using garlic extract for the sensitive and selective enzyme-free detection of ascorbic acid

Abdul Ghaffar Solangi[a], Aneela Tahira[a], Abdul Sattar Chang[b], Tajnees Pirzada[a], Zulfiquar Ali Solangi[j], Fouzia Chang[b], Muhammad Ali Bhatti[h], Adeel Liaquat Bhatti[k], Shusheel Kumar[k], Abdul Hanan[i], Elmuez Dawi[c], Abd Al Karim Haj Ismal[c], Shymaa S. Medany[f], Ayman Nafady[d], L.V. Kangle[g,] Brigitte Vigolo[e], Zafar Hussain Ibupoto[b*]

[a]*Institute of Chemistry, Shah Abdul Latif University Khairpur Mirs, Sindh, Pakistan.* [b]*Institute of Chemistry University of Sindh, Jamshoro, 76080, Pakistan.*

[c]*Nonlinear Dynamics Research Centre (NDRC), Ajman University, P.O. Box 346, United Arab Emirates.*

[d]*Department of Chemistry, College of Science, King Saud University, Riyadh 11451, Saudi Arabia.*

[e]*Université de Lorraine, CNRS, IJL, F-54000 Nancy, France.*

[f]*Department of Chemistry, Faculty of Science, Cairo University, Cairo, Egypt.*

[g]*College of Resource and Environment, South-Central Minzu University, Wuhan 430074, China.*

[h]*Institute of Environmental Sciences, University of Sindh Jamshoro, 76080, Sindh Pakistan.*

[i]*Key Laboratory of Superlight Material and Surface Technology, Ministry of Education, College of Materials Science and Chemical Engineering, Harbin Engineering University, 150001, Harbin, PR China.* [j]*Department of Chemical Engineering, Mehran University of Engineering and Technology, 7680 Jamshoro, Sindh Pakistan.*

[k]*Institute of Physics, University of Sindh Jamshoro, 76080, Sindh Pakistan*

[*]*Corresponding author (s): Zafar Hussain Ibupoto, E-mail: zaffar.ibhupoto@usindh.edu.pk*

Abstract

Low-cost, simple, eco-friendly, environment-friendly, and efficient electroactive materials are highly desirable for a variety of applications, such as energy conversion, energy storage, and non-enzymatic sensing. Our study involved extracting active molecules from garlic green leaf biomass to enhance $NiCo_2O_4$ nanostructures electroactive properties through reducing, stabilizing, and capping agents. Hydrothermally processed different volumes of garlic leaf extract, including 5 mL, 10 mL, and 15 mL, in order to create an optimal electroactive material

based on $NiCo_2O_4$ nanostructures. Characterization of the material based on its morphology, crystallinity, surface chemical composition, and electrochemical testing for enzyme free detection of ascorbic acid (AA) in phosphate buffer solution pH 7.4. The morphology of pure $NiCo_2O_4$ is nanorods which is shifted into nanoparticles due to addition of garlic extract. The advantages of enzyme-free biosensors over enzyme-based biosensors include their ease of manufacture, excellent reproducibility, and stability. The propose to develop highly sensitive and selective non-enzymatic AA sensors based on $NiCo_2O_4$ nanostructures fabricated with garlic leaf extract in a 10 mL volume. The AA sensor presented here operates linearly between 0.5 mM and 8.5 mM with a detection limit of 0.01 mM. An AA sensor has been found to be highly selective, stable, repeatable, and capable of quantifying the concentration of AA in a variety of real-life samples.

Keywords: Garlic leaves extract, $NiCo_2O_4$ nanostructures, Ascorbic acid, Non-enzymatic sensor

1. Introduction

Ascorbic acid (AA) is a micronutrient that plays an important role in organism metabolism and growth. It is also used in the treatment of various diseases, such as scurvy, poisoning, and atherosclerosis [1-3]. Due to the fact that the human body is not able to synthesize AA, it must be ingested from outside sources, such as fresh fruit, vitamin supplements, and beverages containing vitamin C. AA content should be monitored in biological samples, food, and medications to help diagnose diseases, detect illnesses, and promote sustainable consumption [4, 5]. Further, AA must be quantitatively analyzed from samples of foods, pharmaceuticals, and cosmetics [6]. In order to maintain the sustainability of human lives and industrial applications. Several methods, such as solid phase iodine [7], spectrophotometry[8], titrimetric [9], electrophoresis [10], fluorescence [11], chemiluminescence [12] and electrochemical techniques [13] have been applied to quantify AA. An example of high-performance liquid chromatography (HPLC) is the selective detection of several biomolecules in a mixture, but it is more time-consuming, expensive, and labor-intensive than conventional methods [14]. In many cases, these analytical techniques are quite expensive, labor-intensive, and difficult to use. On

the other hand, electrochemical techniques have proven to be straightforward, affordable, extremely sensitive, and selective in recent years, thus they have attracted a great deal of attention [15]. AA has been quantified using two electrochemical methods, including enzyme-based and enzyme-free methods [16]. As enzyme immobilization is expensive and enzyme based biosensors have several problems including denaturation of enzymes during storage, non-enzymatic methods have been utilized extensively as an alternative method to enzyme-based methods for AA detection [17]. The use of high electrocatalytic materials for non-enzymatic methods has always been desired for non-real-time applications with a higher sensitivity and selectivity than electrochemical methods [18]. It is therefore challenging to develop such efficient electrocatalytic materials, but by adapting green chemistry we can overcome this challenge. Numerous electrocatalytic materials have been developed and investigated for non-enzymatic sensors as a result [19]. The strong electrochemical activity of metal oxides makes them suitable for this application [20]. Bimetallic oxides, particularly nickel-cobalt oxides ($NiCo_2O_4$), have been found to be excellent materials for the development of non-enzymatic sensors, owing to their significant redox properties. Since $NiCo_2O_4$ nanostructures have limited surface characteristics and poor electrochemical performance, they have been combined with other materials to develop composites such as $MnO_2/NiCo_2O_4$ [21], Co_3O_4 / $NiCo_2O_4$ [22], $NiCo_2O_4$ @ graphene [23] and Fe_2O_3 @ $NiCo_2O_4$ [24]. Moreover, numerous morphologies of $NiCo_2O_4$ have been fabricated including nanosphere [24], nanorods [21], nanosheets [25] and nanotubes [26]. To design non-enzymatic AA acid sensors with high sensitivity, new methods for improving $NiCo_2O_4$ electrochemical performance must be explored. Due to its eco-friendliness, low cost, and environmental friendliness, green chemistry has received a great deal of attention recently, and it is expected to grow rapidly in the future [23]. A green method of mediation that utilizes biomass waste materials can be used to tailor the surface properties of nanostructured materials, such as the catalytic sites and charge transfer properties [27]. Currently, only a few studies have been conducted on the production of $NiCo_2O_4$ nanostructured materials using biomass wastes. Considering the above facts, outstanding phytochemical analysis of garlic (Allium sativum) leaves extract has been reported for the first time in order to alter the shape and surface properties of $NiCo_2O_4$ with AA being detected in a highly sensitive and selective manner. Garlic (Allium sativum) leaves extract contains several phytochemical compounds, including allicin, alliin, diallyl sulphide, S-allyl-1- cysteine, diallyl disulfide, diallyl

tri sulfide, allyl mercaptan, and (R)-S- (2-hydroxypropyl) cysteine [28]. It has been demonstrated that garlic leaves' (Allium sativum) extract contains phytochemicals that can create surface vacancies and modify the surface chemical events of nanostructured materials. Scheme 1 illustrates the major phytochemicals that can serve as reducing, capping, and stabilizing agents. As part of this study, garlic leaf extract was used as a catalyst during the hydrothermal process to produce $NiCo_2O_4$ nanostructures for use in the robotic determination of AA.

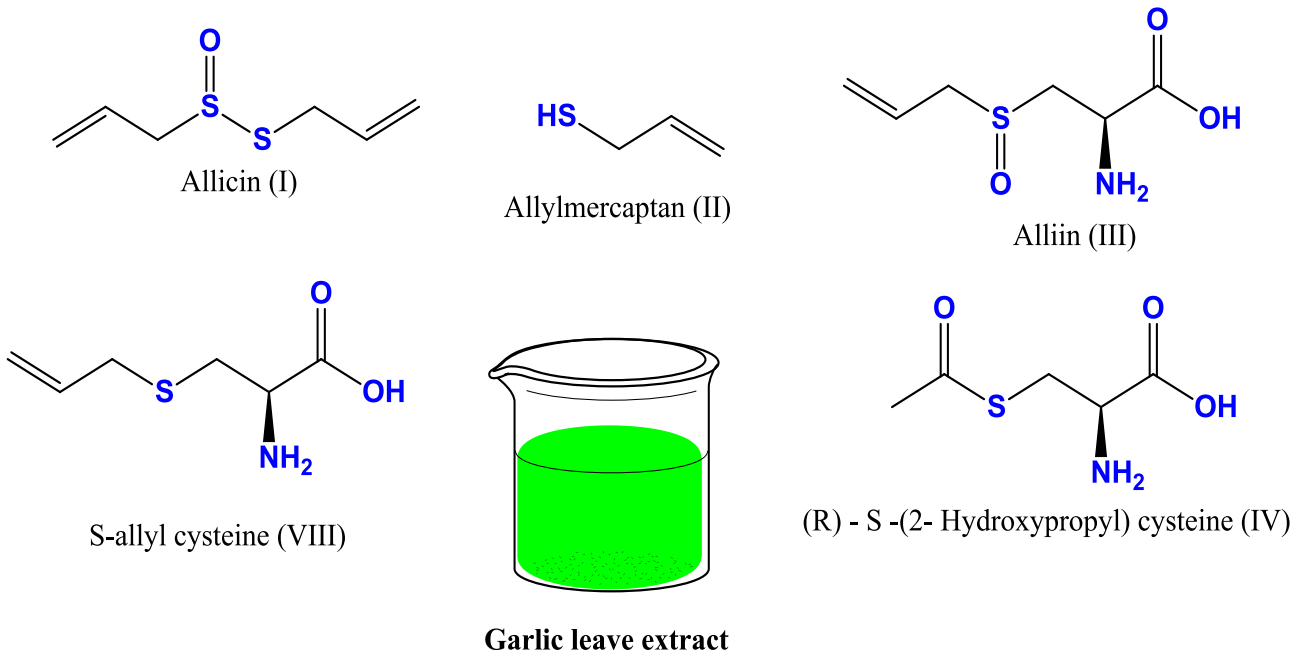

Scheme 1: Shows the various phytochemicals present in the garlic (*Allium sativum*) extract.

2. Experimental Section

2.1. Chemical reagents used

In this study, nickel chloride hexahydrate ($NiCl_2.6H_2O$), cobalt chloride hexahydrate ($CoCl_2.6H_2O$), lactic acid, glucose, sodium chloride, uric acid, potassium chloride, ascorbic acid, glucose, sodium hydroxide, urea, hydrochloric acid, disodium phosphate, and monopotassium

phosphate were used without pretreatment. Chemical reagents were purchased from Sigma

Aldrich, Karachi, and Sindh, Pakistan, and were of analytical grade. During the electrochemical

determination of AA, deionized water was used to prepare the solution and pH 7.4 phosphate buffer solution as the electrolyte medium. The synthesis of $NiCo_2O_4$ nanostructures was carried out by a hydrothermal process in the presence of phytochemicals from garlic leaf extract. Fresh garlic leaves were purchased at the local market, cleaned with deionized water, and allowed to air dry for five hours. In the next step, the garlic leaves are chopped and placed in a juicer to make the extract. In order to produce $NiCo_2O_4$ nanostructures in the presence of garlic leaves extract, 100 mL of deionized water was added, different concentrations of garlic leaf extract, cobalt chloride hexahydrate (0.1M), urea (0.1M) and nickel chloride hexahydrate (0.015M) were added. In order to achieve a pH between 8.2 and 7.4, different volumes of garlic leaf extract (5 mL, 10 mL, and 15 mL) were added to the growth solution. The 100 mL growth solutions were then covered with aluminum sheets and hydrothermal reactions were conducted at 95 °C for five hours. The nickel-cobalt bimetallic hydroxide phase material was recovered on the filter paper and repeatedly rinsed with deionized water. After collecting the hydroxide phase, it was dried at room temperature for 12 hours. Material was thermally burned for five hours at 500 °C in the open air. Using the same method, pure $NiCo_2O_4$ nanostructures were synthesized without the use of garlic leaf extract. Finally $NiCo_2O_4$ nanostructured obtained possess black color which is

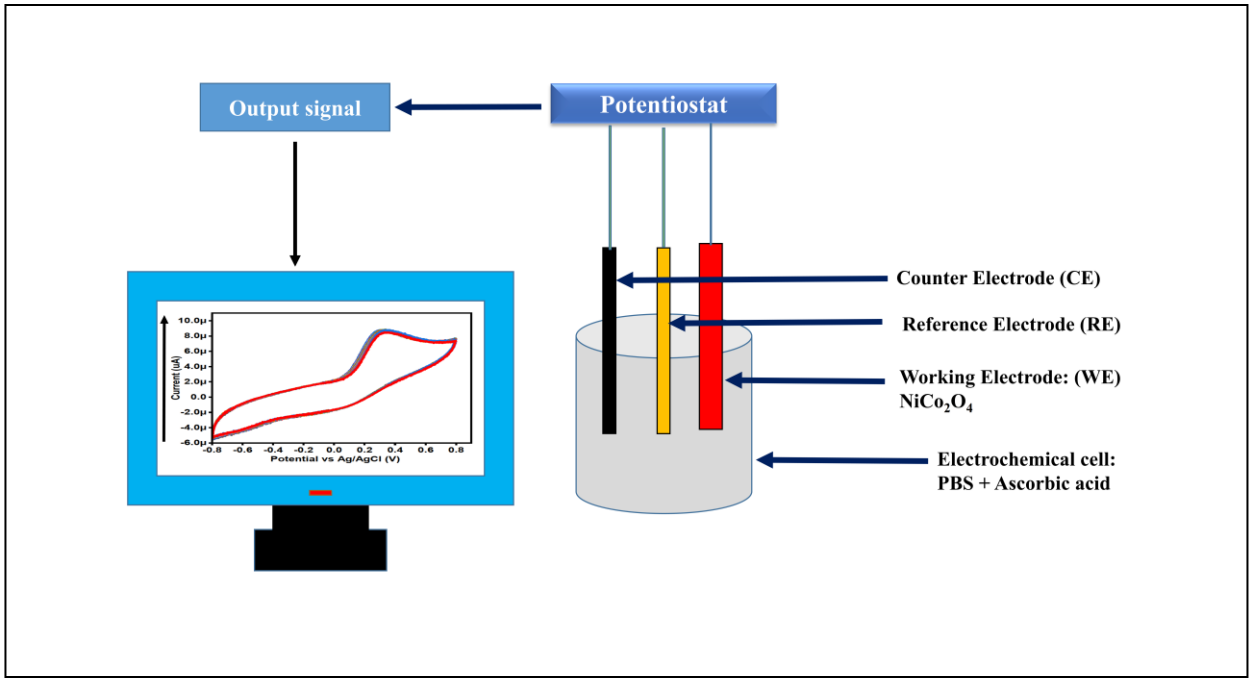

preserve for further analysis.

Scheme 2. A, schematic of a typical $NiCo_2O_4$ nanomaterial cyclic voltammetric electrochemical sensor composed of a carbon based working electrode (WE), reference electrode (RE) and counter electrode (CE).

2.2. Physical investigations of different $NiCo_2O_4$ nanostructures

SEM (JEOL Japan Model No. JSM-IT 100, Auto Fine Coater: JEC-3000FC, Coating done on a 20 mA current for 60 seconds), employing an accelerating voltage of 10 kV, was used to investigate the morphology of $NiCo_2O_4$ nanostructures. We used powder X-ray diffraction (XRD) to analyze the crystal quality of garlic leaves extract $NiCo_2O_4$ nanostructures at 45 kV and 45 mA using CuK radiation (λ=1.5418 Å) as a source of X-rays. A 200 kV high resolution transmission electron microscope (HRTEM) was used to examine the confined nanoscale structure. The elemental mapping was quantified using energy dispersive spectroscopy. Chemical valence states were confirmed by X-ray photoelectron spectroscopy (XPS) under extremely high vacuum. A Shirley type background and Voigt curves were used to deconvolve the XPS features using C1s at 284.6 eV as the reference binding energy.

2.3. Non-enzymatic sensing of AA onto surface modified $NiCo_2O_4$ nanostructures

Various electrochemical techniques have been used to characterize non-enzymatic AA sensors, including cyclic voltammetry, amperometry, electrochemical impedance spectroscopy, and linear sweeping voltammetry. This experiment was conducted with a three-electrode configuration, consisting of silver-silver chloride (Ag/AgCl, filled with 3.0 M KCl) serving as the reference electrode, platinum sheet serving as the counter electrode, and glassy carbon electrode (GCE) as the working electrode. Before modification, the GCE was washed with deionized water and polished with alumina paste (0.3µm) and silicon paper. An ink containing ten mg of $NiCo_2O_4$ nanostructures and 0.5 mL of Nafion (5%) was prepared using 2.5 m of deionized water and 0.5 mL of Nafion. We prepared a 10 mM stock solution of AA in 0.1 M phosphate buffer solution at pH 7.4. The AA was dissolved in a buffer solution of phosphate buffer. We prepared new AA solutions by diluting them in buffer solutions containing potassium ions, potassium ions, and sodium ions at pH 7.4 in order to analyze the selectivity of non-enzymatic AA sensors. A non-enzymatic AA sensor's selectivity was tested using 0.1 mM interfering species, including urea,

lactic acid, glucose, uric acid, potassium ions, and sodium ions, at the same concentration of AA. To determine the linear range of the AA sensor, different concentrations of AA were dissolved in 0.1M phosphate buffer solution (PBS), pH 7.4, using CV and chronoamperometry methods. Using this technique, the low limit of detection of a non-enzymatic sensor could be estimated [29]. Synthesis, electrochemical signal and the general ascorbic acid sensing mechanism is shown in Scheme 2.

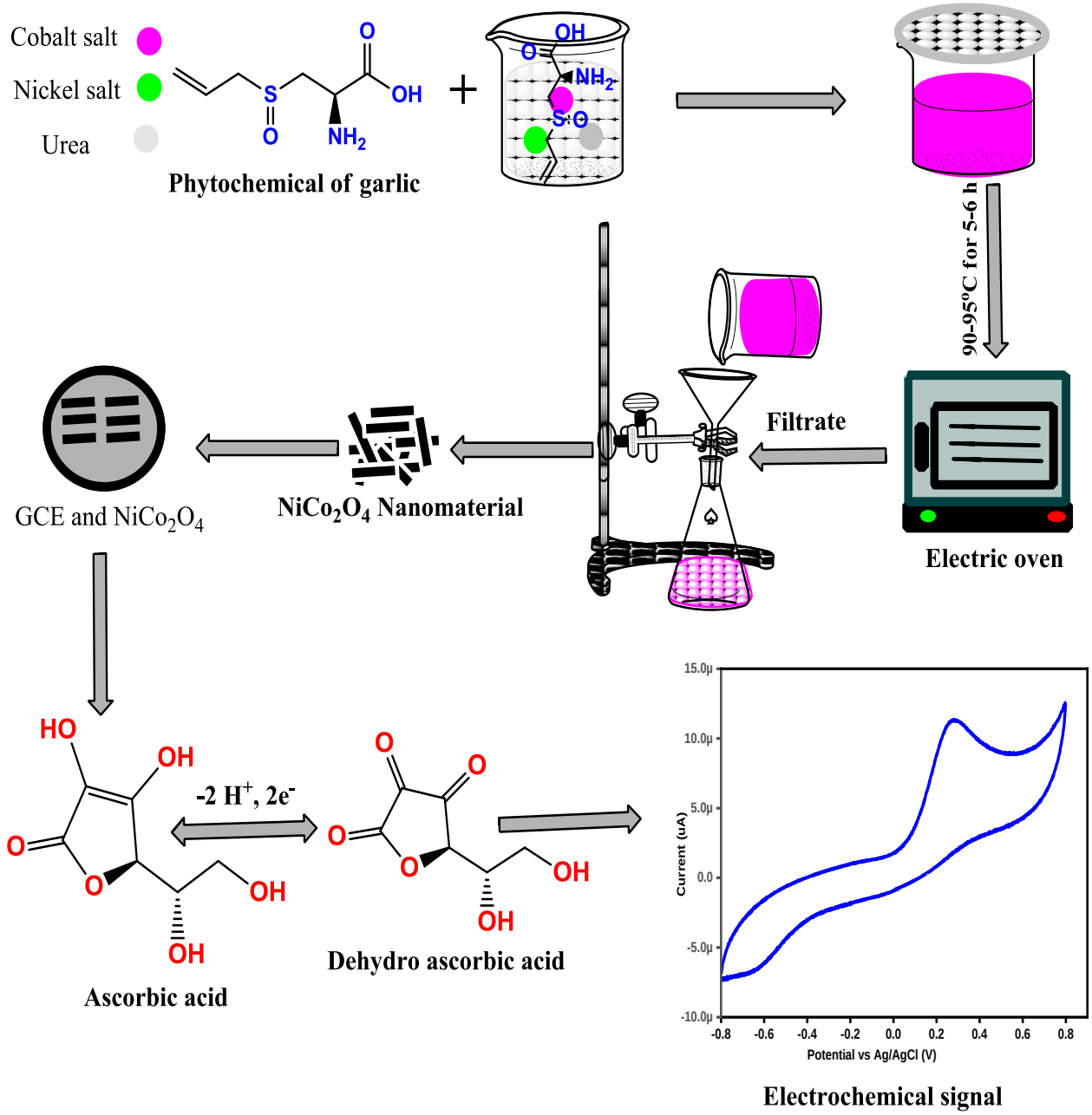

Scheme 2: Stepwise synthesis of $NiCo_2O_4$ nanostructures using garlic leaves extract and general oxidation mechanisms of AA using electroanalytical method.

3. Results and discussion

3.1. Structural and morphological investigations of garlic leaves extract assisted different $NiCo_2O_4$ nanostructures

Figure 1 illustrates the diffraction patterns obtained from powder XRD measurements of $NiCo_2O_4$ nanostructures used to evaluate crystal quality. In addition, phytochemicals from garlic leaf extract have been observed to have a positive effect on the crystal quality of $NiCo_2O_4$ nanostructures. A good match was found between the measured diffraction patterns and the standard JCPDS card no: 96-900-5891, attesting a cubic crystal phase of the material and confirming the high purity of the preparation in the presence of garlic leaf extract. Typical $NiCo_2O_4$ nanostructure reflections are (111), (220), (311), (222), (400), (511) and (440), at two theta angles 19.40, 31.30, 36.880, 38.590, 44.850, 59.410, and 65.300, respectively. The crystal cubic phase and composition of $NiCo_2O_4$ nanostructures were not altered by garlic leaf extract; however, the relative intensities were slightly varied as a result of the reducing, capping, and stabilizing properties of the phytochemicals of garlic leaves extract, which can be attributed to these properties as shown in Figure 1. In Figure 2a-e, $NiCo_2O_4$ nanostructures were examined using SEM to determine their shape. In Figure 2a, a pure $NiCo_2O_4$ nanostructure exhibits a nanorod-like morphology with dimension of several microns in length. Garlic leaf extract changed the morphology of $NiCo_2O_4$ nanostructures, changing them from nanorods to short-range nanoparticles as shown in Figures 2b–e, indicating the impact of phytochemicals on the surface morphology. Based on Figure 2e, $NiCo_2O_4$ nanostructures obtained with garlic leaf extract are typically in the nanoscale dimension of 50-100 nm, confirming the role of capping, reducing, and stabilizing agents. $NiCo_2O_4$ nanostructures may be structurally modified by phytochemicals contained in garlic leaf extract. As shown in Scheme 1, the transition from nanorods to nanoparticles was caused by the presence of terminated oxygenated groups

originating from phytochemicals in garlic leaf extract. The phytochemicals are molecules with reducing, capping, and stabilizing properties that played a vital role during growth and transformed the morphology from nanorods to nanoparticles. HRTEM and fast Fourier transform (FFT) images were taken using Image J software to examine the deep morphological features of $NiCo_2O_4$ nanostructures and calculate d-spacing at the atomic level. HRTEM analysis was performed on pristine $NiCo_2O_4$ nanostructures and garlic leaves extract of 10 mL assisted synthesized $NiCo_2O_4$ nanostructures as shown in Figure 3 and 4. Figure 3 shows the first TEM/HRTEM analysis, elemental mapping, and EDS spectra for pure $NiCo_2O_4$ nanostructures. Nevertheless, the d-spacing values were calculated using Image-J software According to Figure 3(a), the calculated d-spacing value for pristine materials is 0.46 nm [30, 31]. For further verification, the EDS spectra and elemental mapping of pristine material are shown in Fig 3 (b-e). Moreover, the $NiCo_2O_4$ nanostructures prepared with 10 mL of garlic leaves extract have shown a reduction in d-spacing compared to the pure $NiCo_2O_4$ nanostructures, as shown in Figure 4 (a), along with the desired FFT transformation [32, 33]. In Figure 4(b, c, d, and e), the elemental mapping along with corresponding EDS spectra are illustrated. As a result of the reduction in d-spacing values of the desired material, phytochemicals from garlic leaves have demonstrated the successful role of reducing, coloring and stabilizing agents. A study of the synthetic garlic leaves extract has demonstrated the presence of more active sites, vacancies, and possible electrochemical activity towards facilitating electron transfer between electrodes [34].

In addition, we performed the XPS measurements as shown in Figure 5 in order to gain a better understanding of the chemical states and surface species of $NiCo_2O_4$ nanostructures prepared with garlic leaves extract. The synthesis process for $NiCo_2O_4$ nanostructures without garlic leaves extract is similar to that used here, thus pristine $NiCo_2O_4$ nanostructures have been reported previously [70], both without and with garlic leaves extract. An average binding energy for carbon was determined based on the XPS binding energies of each element. According to Figure 5a, there are two different chemical states of Co in $NiCo_2O_4$ nanostructures. According to Figure 5a, there are two spin orbital peaks located 779.73 eV and 781.60 eV, respectively, corresponding to the two oxidation states of Co^{3+} and Co^{2+}. Additionally, two satellite peaks were observed in the resolved Co 2p spectrum at 785.8 eV and 789.37 eV. We calculated the relative percentages of Co^{3+} and Co^{2+} to be 60.18% and 27.29%, respectively. Figure 5b shows the Voigt fitting for the Ni 2p spectrum. Similarly, Ni^{2+} and Ni^{3+} valence states were found to

have two spin orbital double peaks at 853.88 eV and 855.60 eV, respectively, as shown in Figure 5b. A relative percentage of Ni^{2+} and Ni^{3+} valence is 6.06% and 67.38%, respectively. Satellite peak was identified at 861.34 eV with a relative percentage of 25.96%. It has been shown that XPS fits for Ni 2p are in agreement with those in previous studies [21, 35]. Moreover, the O 1s spectrum of $NiCo_2O_4$ nanostructures prepared with 10 mL of garlic leaf extract was collected, and its fitting results are shown in Figure 5c. We have determined that the binding energies estimated at 529.69 eV, 531.10 eV, and 532.68 eV for well resolved three peaks have been associated with distinct metal-oxygen, oxygen ions, and physic/chemisorbed water on the surface of $NiCo_2O_4$ nanostructures, and these results are consistent with earlier publications [35]. According to the published studies, $NiCo_2O_4$ nanostructures prepared with garlic leaves extract have high oxygen ions (O^-) and Co^{3+} valence states that are highly favorable for electrocatalytic reactions [21].

3.2. Non-enzymatic sensing of ascorbic acid (AA) using $NiCo_2O_4$ nanostructures prepared with garlic leaves extract

A phosphate buffer solution of pH 7.4 has been used as an electrolyte for the development of AA sensors. The detection of AA was carried out using a three-electrode cell circuit. As can be seen in Figure 6a, cyclic voltammetry was employed to obtain preliminary electrochemical signals for each electrode. We modified four GCEs with pure $NiCo_2O_4$ nanostructures and three samples of $NiCo_2O_4$ nanostructures prepared with 5 mL, 10 mL, and 15 mL of garlic leaves extract. In Figure 6a, CV curves were recorded at a scan rate of 50 mV/s using a 0.5mM AA concentration. In Figure 6a, it is evident that $NiCo_2O_4$ nanostructures prepared with 10 mL of garlic leaves extract show strong oxidation signals compared to pristine $NiCo_2O_4$ nanostructures. The electrochemical performance of $NiCo_2O_4$ nanostructures was enhanced by 5 mL of garlic leaf extract, while the optimum concentration of nanostructured material was observed with 10 mL of garlic leaf extract. Further addition of garlic leaves extract has drastically decreased the effectiveness of $NiCo_2O_4$ nanostructures, which may be attributed to a decrease in active sites. The surface of the material became less active, and there were favorable features on the surface that could enhance the AA oxidation, thus a 15 mL use of garlic leaves extract has been found as the limiting factor in demonstrating $NiCo_2O_4$ nanostructures' functionality. It is shown in Figure 6b that $NiCo_2O_4$ nanostructures and bare glassy carbon electrodes were tested in the presence and

absence of 0.5 mM AA in a phosphate buffer solution at pH 7.4. $NiCo_2O_4$ nanostructures are assumed to have generated the signal primarily for AA, whereas the bare glassy carbon electrode, as shown in Figure 6b, did not demonstrate any electrochemical activity. As a result of this preliminary testing, systematic sensor studies were conducted using $NiCo_2O_4$ nanostructures prepared with 10 mL of garlic leaves extract. Using $NiCo_2O_4$ nanostructures, the CV study has demonstrated the possibility of detecting AA using the following mechanism. In typical electron transfer reactions, Co^{3+} and Ni^{3+} ions were given electrons by oxidizing AA and reduced to Co^{2+} and Ni^{2+}. The enhanced oxidation signal of $NiCo_2O_4$ nanostructures synthesized with 10 mL of garlic leaves extract could be attributed to high density of active sites exposure, favorable charge transfer at the interface of electrode and electrolyte, and unique morphological characteristics tuned by the reducing, capping and stabilizing agents from phytochemicals of garlic leaves extract. Electrode kinetics of $NiCo_2O_4$ nanostructures prepared with 10 mL of garlic leaves extract was explored by CV study using 0.5 mM AA solution at different scan rates as shown in Figure 7a. An increase in scan rate resulted in a linear increase in oxidation peak current, thus demonstrating diffusion-controlled kinetics for the electrochemical reaction of AA. Figure 7b shows the oxidation peak currents of each scan rate plotted against the square root of the scan rate, and these findings are fully supported by the literature [35-38]. There was a regression coefficient of 0.99 during the scan rate study in the presence of AA oxidation, which was regulated by surface adsorption and electrochemistry [38, 39]. Our study investigated the influence of pH on the oxidation process of AA and obtained results through CV curves at different pH values adjusted in 0.5 mm of AA are shown in Figure 8a. A nonenzymatic AA sensor was evaluated at pH 7.4 because the shape and current of the peaks are more apparent. As a result of the pH investigation, it was found that the pH of the analyte solution significantly influenced the activity of $NiCo_2O_4$ nanostructures, and these aspects have already been reported previously [39]. There has been a significant effect on the limited activity of $NiCo_2O_4$ nanostructures as shown in Figure 8b, which is pH dependent. This indicates that analytes with pH close to 7.4 experience favorable oxidation of AA; however, analytes with pH below or above 7.4 may be less effective and less stable. Such phenomena have been well documented before [40]. Upon analyzing the pH ranges of 5.4, 6.4, 7.4, 8.4 and 9.4, it is verified that the CV results shown are highly stable at pH 7.4 and show an enhanced oxidation peak, therefore all electrochemical experiments were conducted at pH 7.4.

$NH_2CONH_2 + H_2O \longrightarrow 2NH_3 + CO_2$.....(Eq. 1)

$NH_3 + H_2O \longrightarrow NH_4^+ + OH^-$.....(Eq. 2)

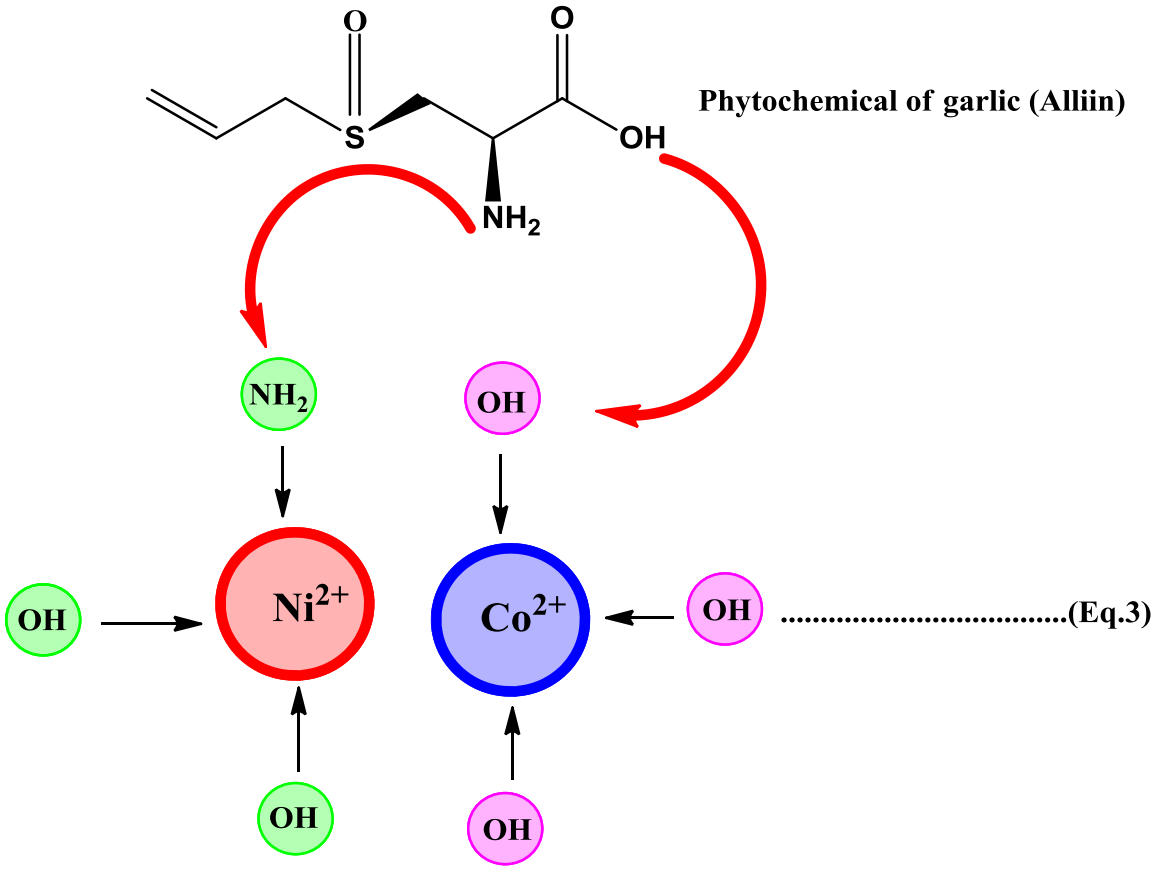

.....(Eq.3)

$Ni^{2+} + 2Co^{2+} + 6OH^- \longrightarrow [NiCo_2(OH)_6]$.....(Eq. 4)

$[NiCo_2(OH)_6] + 1/2\ O_2 \longrightarrow NiCo_2O_4 + 3H_2O$.....(Eq. 5)

3.3. The calibration plots, stability, repeatability and selectivity studies of newly developed non-enzymatic AA sensor based on surface modified $NiCo_2O_4$ nanostructures.

An examination of the linear range of AA detection and the limit of detection was conducted using $NiCo_2O_4$ nanostructures prepared with 10 mL of garlic leaves extract. In order to maintain the sensing range, different electrochemical modes were employed, and based on the sensitivity

of each electrochemical mode, we observed different AA linear ranges for $NiCo_2O_4$ nanostructures prepared with 10 mL of garlic leaves extract. As a first step, the linear range of AA at several concentrations in phosphate buffer solution at pH 7.4 was determined by CV at 50 mV/s using a range of concentrations of AA in phosphate buffer solution. According to Figure 9a, the peak current for AA oxidation increased linearly with increasing AA concentrations, and the linear range of AA was found to range between 0.5 and 8.5 mM. Based on the results of this study, it appears that AA non-enzymatic sensors have shown a wide linear range among those that have been reported thus far [41-46]. In addition, the linear plot depicted in Figure 9b was constructed by selecting the oxidation peak current for each AA concentration against different AA concentrations in order to assess the analytical quality of a newly constructed non-enzymatic AA sensor in terms of accuracy and precision. Based on the linear plot of CV data, AA sensors can quantify a wide range of AA concentrations and can be applied to analysis of real samples. A limit of detection (LOD) and a limit of quantification (LOQ) were estimated based on published research [41]. It was determined that the LOD and LOQ in this study were 0.01 mM and 0.04 mM, respectively. The reported results shown in Table 1 based on the non-enzymatic AA, it is very much clear that the suggested approach to AA analysis could prove very valuable as a substitute technique for AA detection in real samples where a broad linear range and a low detection limit are highly desirable. Additionally, the linear sweep voltammetry (LSV) mode was used to estimate the calibration of a newly constructed non-enzymatic AA sensor, with the results shown in Figure 10a. Fig. 10a illustrates how the proposed AA sensor arrangement can detect AA over a wide linear range, from 0.1mM to 7.0mM and generate a measurable amount of current. In the case of LSV measurements, as the concentration of AA increases, a greater current is produced, demonstrating the sensitivity of the recently designed AA sensor. In Figure 10b, a linear plot of peak current against different concentrations of AA is shown. Based on a linear fitting of LSV curves, the proposed non-enzymatic AA sensor exhibits outstanding analytical performance and has a coefficient of 0.99 as a regression coefficient. An AA sensor based on a full CV curve can detect a wide linear range of AA with a precise and accurate output based on full CV curves as well as half CV curves. As shown in Figure 11a, the linear range of the AA sensor was also calculated using the extremely sensitive electrochemical mode of amperometry. As long as the concentration of AA was between 0.5 mM and 3.5 mM, the amperometric signal was highly sensitive. The figure 11b shows a linear plot of the

amperometric signal for these various AA concentrations. A regression coefficient of 0.99 confirms the good performance of the AA detection with powerful analytical features. Several factors have contributed to the outstanding electrochemical activity of $NiCo_2O_4$ nanostructures prepared with 10 mL garlic leaf extract, including oxygen vacancies on the surface, good crystal quality, surface modification by reducing agents, and well-controlled size and shape due to the capping agent and stabilizing agents from garlic leaf extract phytochemicals. It has been confirmed by a variety of analytical techniques such as SEM, XRD, HRTEM, and XPS. A selectivity experiment was performed to determine the performance of the proposed AA sensor in the presence of potential interfering species during the detection of AA. With CV curves at 50 mV/s in 0.5mM AA, we have used a variety of interfering species such as glucose, uric acid, urea, lactic acid, mannose, sodium ions, chloride ions, potassium ions, and calcium ions, as shown in Figure 12a. In terms of oxidation peak position, drift in oxidation potential, and peak current, AA sensor was found to be unaffected by successive additions of interfering species in the presence of AA. According to this study, the proposed AA sensor configuration has excellent selectivity and may be suitable for the detection of AA in biological matrixes. A bar graph is depicted in Figure 12b showing the peak current variation of AA following the addition of interfering species. The change in peak current is less than 4%. By reducing, capping, and stabizling the phytochemicals of garlic leaves extract, $NiCo_2O_4$ nanostructures can be used to selectively quantify the AA even in the presence of competing interfering agents. The repeatability and stability of the modified AA sensor electrode were evaluated by measuring 20 CV cycles at a scan rate of 50 mV/s in 0.5 mM. In Figure 13a, it can be seen that the gadget is capable of being used repeatedly. The stability of AA biosensors is problematic, particularly with regard to enzymatic biosensors. Consequently, we have developed a non-enzymatic AA sensor for practical sample analysis. Figure 13b shows a bar graph of peak current following multiple repeatable CV cycles. As demonstrated by an error rate of less than 5%, the presented approach has excellent analytical properties and reveals that $NiCo_2O_4$ nanostructures do not alter surface features, therefore they can be employed for long-term use. Our study tested the stability of $NiCo_2O_4$ nanostructures in a 0.5 mM AA solution by measuring the amperometric response over a period of 1000s. The results of the amperometry are shown in Figure 14a. As can be observed from the fact that no current fluctuation was observed during the testing, the current AA sensor is appropriate for long-term applications. A wide linear range, a low limit of detection, low

fabrication cost, and simple electroactive material synthesis contributed to the improved performance compared to other reported AA sensors/biosensors in the literature. We conducted electrochemical impedance spectroscopy (EIS) using a sweeping frequency range of 100 kHz to 1 Hz, an amplitude of 10 mV, and a bias potential of 0.4 V in order to support improved electrochemical performance of $NiCo_2O_4$ nanostructures. Nyquist plots were measured for three samples of $NiCo_2O_4$ nanostructures, including the virgin sample, sample 1 and sample 2 in 0.5mM AA. Based on the Nyquist plots for sample 2, the low arc indicates a fast charge transfer between the $NiCo_2O_4$ nanostructured working electrode and the 0.5mM analyte solution, and the intercept of the semicircle on the Nyquist plot at high frequency indicates the electrolyte resistance [47]. It is evident from Nyquist plots that the pristine $NiCo_2O_4$ nanostructures, samples 1 and 3, are limited by poor charge transfer.

3.4. Method of preparation real sample and their analysis

For practical applications, it is crucial to examine the fabrication of the electrode's performance during analysis of real samples. In order to validate the practical application of the sensor for the detection of AA, commercial orange juice was purchased from a nearby market (in Sindh, Pakistan) and tested. It was necessary to filter the sample until clear liquid was obtained in order to remove pulps and suspended particles. We added 10 mL of filtered juice to a 25 mL solution of PBS at a pH of 7.4. The results are shown in Table 2. The results were further confirmed by a standard recovery method. In order to determine AA levels in real samples, ce-cone chewable tablets, which contain vitamin C, were selected as the detection method. We obtained chewable ce-cone tablets from a nearby drugstore. Crushed vitamin C chewable pills (500 mg/tablet) were mixed in 10.0 mL of PBS 0.1 M, pH 7.4. After mixing, the mixture was centrifuged at 13,000 rpm for 20 minutes. To prepare the stock solution for the vitamin C chewable pills, 100 mL of supernatant was diluted to 10.0 mL of ultrapure water. The standard addition method was used to determine the AA content of the Cecone tablet stock solution, and the recoveries were calculated to evaluate the method's accuracy. Results of the percent recovery were highly encouraging for the potential application of $NiCo_2O_4$ nanostructures prepared with 10 mL garlic leaves extract for the detection of AA in the future. Garlic leaves have altered surface properties due to exposure to high density active sites. By promoting charge transfer at the interface, $NiCo_2O_4$ nanostructures can exhibit excellent sensing performance due to their high electrode compatibility.

4. Conclusions

The $NiCo_2O_4$ nanostructures were produced by hydrothermal synthesis of garlic leaf extract. Various volumes of garlic juice were used to prepare optimized electroactive materials based on $NiCo_2O_4$ nanostructures, such as 5 mL, 10 mL, and 15 mL. An analysis of the shape, crystal quality, surface chemical composition, and elemental composition of the material has been conducted. A garlic leaf extract exhibited the potential for phytochemical properties such as reducing, capping and stabilizing agents, which strongly altered surface properties of $NiCo_2O_4$. By using a non-enzymatic sensing approach, the optimized $NiCo_2O_4$ nanostructures with 10 mL garlic leaves extract were found to be highly sensitive toward the detection of AA. The presented AA sensor exhibits a wide linear range between 0.5 mM and 8.5 mM with a low detection limit of 0.01 mM. A proposed AA sensor was tested for stability, repeatability, and selectivity. Because garlic leaves are biomass waste, they offer a variety of useful molecules for tuning and preparing highly electroactive materials for energy conversion, storage, and biomedicine.

Author's contribution

Abdul Ghaffar Solangi, did the material synthesis and evaluate the preliminary sensor performance

Aneela Tahira, did the XRD and analyzed the results

Abdul Sattar Chang, did in depth sensor performance of as prepared materials

Tajnees Pirzada, did the partial supervision

Zulfiquar Ali Solangi, did the EDS analysis and preview the draft of manuscript

Fouzia Chang, did the EIS analysis

Muhammad Ali Bhatti, did the SEM analysis

Adeel Liaquat Bhatti, did real sample analysis

Shusheel Kumar, analyzed the electroanalytical results

Abdul Hanan, did TEM and HRTEM analysis

Elmuez Dawi, did the editing of draft and preview of the analyzed results

Shymaa S. Medany, did mechanism analysis based CV data

Ayman Nafady, did proofreading and validate the electrochemical results

Kangle LV,' did HRTEM and XPS measurements

Brigitte Vigolo, did XPS analysis and proofread the paper

Zafar Hussain Ibupoto, did main supervision, wrote the first draft and preview obtained results

Acknowledgments

The authors would like to gratefully acknowledge the Higher Education Commission Pakistan for partial support under the project NRPU/8350. We also extend our sincere appreciation to the Researchers Supporting Project Number (RSP2023R79) at King Saud University, Riyadh, Saudi Arabia. Brigitte Vigolo would like to thank the platform "Microscopies, Microprobes and Metallography (3 M)" (Institut Jean Lamour, IJL, Nancy, France) for access to SEM facilities and F. Alnjiman for his valuable help. Authors would also like to acknowledge partial funding of the Ajman University, Grant ID: DGSR ref. 2022-IRG-HBS-5.

Conflict of Interest

Authors declare no competing interests in the resented research work

5. References

[1] Li M, Zhang S, Li H, Chen M (2023) Cerium/polyacrylic acid modified porphyrin metal-organic framework as fluorescence and photothermal sensor for ascorbic acid measurement.Talanta 252: 123825.

[2] Kim WS, Dahlgren RL, Moroz LL, Sweedler JV (2002) Ascorbic acid assays of individual neurons and neuronal tissues using capillary electrophoresis with laser-induced fluorescence detection. Analytical chemistry 74: 5614.

[3] Bohndiek SE, Kettunen MI, Hu DE, Kennedy BW, Boren J, Gallagher FA, Brindle .M (2011) Hyperpolarized [1-13C]-ascorbic and dehydroascorbic acid: vitamin C as a probe for imaging redox status in vivo. Journal of the American Chemical Society 133: 11795.

[4] Luo X, Zhang W, Han Y, Chen X, Zhu L, Tang W, Wang J, Yue T, Li Z (2018) N, S co-

doped carbon dots based fluorescent “on-off-on” sensor for determination of ascorbic acid in common fruits. Food chemistry 258: 214.

[5] Liu R, Yang R, Qu C, Mao H, Hu Y, Li J, Qu L (2017) Synthesis of glycine-functionalized graphene quantum dots as highly sensitive and selective fluorescent sensor of ascorbic acid in human serum.. Sensors and Actuators B: Chemical 241: 644.

[6] Valdramidis V, Cullen PJ, Tiwari B, O’Donnell CP (2010) Quantitative modelling approaches for ascorbic acid degradation and non-enzymatic browning of orange juice during ultrasound processing. Journal of Food Engineering 96: 449.

[7] Noroozifar M, Khorasani-Motlagh M (2003) Solid-phase iodine as an oxidant in flow injection analysis: determination of ascorbic acid in pharmaceuticals and foods by background correction. Talanta 61: 173.

[8] Jain A, Chaurasia A, Verma KK (1995) Determination of ascorbic acid in soft drinks, preserved fruit juices and pharmaceuticals by flow injection spectrophotometry: Matrix absorbance correction by treatment with sodium hydroxide.Talanta 42: 779.

[9] Arya S, Mahajan M, Jain P (2000) Non-spectrophotometric methods for the determination of Vitamin C. Analytica Chimica Acta 417: 1.

[10] Tang Y, Wu M (2005) "A quick method for the simultaneous determination of ascorbic acid and sorbic acid in fruit juices by capillary zone electrophoresis." Talanta 65: 794.

[11] Perez-Ruiz T, Martinez-Lozano C, Tomas V, Fenol J (2001) Fluorimetric determination of total ascorbic acid by a stopped-flow mixing technique. Analyst 126: 1436.

[12] Bijad M, Karimi-Maleh H, Khalilzadeh MA (2013) Application of ZnO/CNTs nanocomposite ionic liquid paste electrode as a sensitive voltammetric sensor for determination of ascorbic acid in food samples. Food Analytical Methods 6: 1639.

[13] Pachla LA, Kissinger PT (1976) "Determination of ascorbic acid in foodstuffs, pharmaceuticals, and body fluids by liquid chromatography with electrochemical detection." Analytical Chemistry 48: 364.

[14] Lykkesfeldt J (2000) Determination of ascorbic acid and dehydroascorbic acid in biological samples by high-performance liquid chromatography using subtraction methods: reliable reduction with tris [2-carboxyethyl] phosphine hydrochloride. Analytical biochemistry 282: 89.

[15] Sha R, Badhulika S (2018) Facile green synthesis of reduced graphene oxide/tin oxide composite for highly selective and ultra-sensitive detection of ascorbic acid. Journal of Electroanalytical Chemistry 816: 30.

[16] Özcan A, Şahin Y (2010) "Preparation of selective and sensitive electrochemically treated pencil graphite electrodes for the determination of uric acid in urine and blood serum." Biosensors and Bioelectronics 25: 2497.

[17] Wayu MB, Schwarzmann MA, Gillespie SD, Leopold MC (2017) Enzyme-free uric acid electrochemical sensors using β-cyclodextrin-modified carboxylic acid-functionalized carbon nanotubes. Journal of materials science 52: 6050.

[18] J. Wang, B. Yang, J. Zhong (2017) "Dopamine and uric acid electrochemical sensor based on a glassy carbon electrode modified with cubic Pd and reduced graphene oxide nanocomposite," Journal of colloid and interface science 172-180.

[19] Ding R, Qi L, Jia M, Wang H (2014) Facile synthesis of mesoporous spinel NiCo 2 O 4 nanostructures as highly efficient electrocatalysts for urea electro-oxidation. Nanoscale 6: 1369.

[20] Zhang G, Wang T, Yu X, Zhang H, Duan H, Lu B (2013) Nanoforest of hierarchical Co3O4@ NiCo2O4 nanowire arrays for high-performance supercapacitors. Nano Energy 2: 586.

[21] Jokar E, Zad AI, Shahrokhian S (2015) Synthesis and characterization of NiCo 2 O 4 nanorods for preparation of supercapacitor electrodes. Journal of Solid State Electrochemistry 19: 269.

[22] Huang G, Zhang L, Zhang F, Wang L, (2014) Metal–organic framework derived Fe 2 O 3@ NiCo 2 O 4 porous nanocages as anode materials for Li-ion batteries. Nanoscale 6: 5509.

[23] He Q, Liu J, Liu X, Chen D, Deng P, Liang J (2018) Fabrication of amine-modified magnetite-electrochemically reduced graphene oxide nanocomposite modified glassy carbon electrode for sensitive dopamine determination. Nanomaterials 8: 194.

[24] Zhou Y, Ma L, Gan M, Ye M, Li X, Zhai Y, Yan F, Cao F (2018) Monodisperse MnO2@ NiCo2O4 core/shell nanospheres with highly opened structures as electrode materials for good-performance supercapacitors. Applied Surface Science 444: 1.

[25] Xu K, Yang X, Yang J, Hu J (2017) Synthesis of hierarchical Co3O4@ NiCo2O4 core-shell nanosheets as electrode materials for supercapacitor application. Journal of Alloys and Compounds 700: 247.

[26] Chu Q, Yang B, Wang W, Tong W, Wang X, Liu X, Chen J (2016) Fabrication of a Stainless-Steel-Mesh-Supported Hierarchical Fe2O3@ NiCo2O4 Core-Shell Tubular Array Anode for Lithium-Ion Battery. ChemistrySelect 1: 5569.

[28] Nawaz H, Shad MA, Rauf A (2018) "Optimization of extraction yield and antioxidant properties of Brassica oleracea Convar Capitata Var L. leaf extracts." Food Chemistry 242: 182.

[29] Amin S, Tahira A, Solangi AR, Mazzaro R, Ibupoto ZH, Fatima A, Vomiero A (2020) Functional nickel oxide nanostructures for ethanol oxidation in alkaline media. Electroanalysis 32: 1052.

[30] Hanan A, Ahmed M, Lakhan MN, Shar AH, Cao D, Asif A, Ali A, Gul M (2022) "Novel rGO@ Fe3O4 nanostructures: An active electrocatalyst for hydrogen evolution reaction in alkaline media." Journal of the Indian Chemical Society 99: 100442.

[31] Gong M, Zhou W, Tsai MC, Zhou J, Guan M, Lin MC, Zhang B, Hu Y, Wang DY, Yang J, Pennycook SJ (2014) Nanoscale nickel oxide/nickel heterostructures for active hydrogen evolution electrocatalysis. Nature communications 5: 4695.

[32] Lim TH, Cho SJ, Yang HS, Engelhard MH, Kim DH (2015) "Effect of Co/Ni ratios in cobalt nickel mixed oxide catalysts on methane combustion." Applied Catalysis A: General 505: 62.

[33] Ahsan MT, Usman M, Ali Z, Javed S, Ali R, Farooq MU, Akram MA, Mahmood A (2020) "3D hierarchically mesoporous zinc-nickel-cobalt ternary oxide (Zn0. 6Ni0. 8Co1. 6O4) nanowires for high-performance asymmetric supercapacitors." Frontiers in chemistry 8: 487.

[34] Li H, Cai C, Wang Q, Chen S, Fu J, Liu B, Hu Q, Hu K, Li H, Hu J, Liu Q (2022) "High-performance alkaline water splitting by Ni nanoparticle-decorated Mo-Ni microrods: Enhanced ion adsorption by the local electric field." Chemical Engineering Journal 435: 134860.

[35] A Hanan, D Shu, U Aftab, Cao D, Laghari AJ, Solangi MY, Abro MI, Nafady A, Vigolo B, Tahira A, Ibupoto ZH (2022) Co2FeO4@ rGO composite: Towards trifunctional water splitting in alkaline media. International Journal of Hydrogen Energy 47: 33919.

[36] Li W, Zhang B, Lin R, et al. (2018) "A dendritic nickel cobalt sulfide nanostructure for alkaline battery electrodes." Advanced Functional Materials 28: 1705937.

[37] López-Tinoco J, Mendoza-Cruz R, Bazán-Díaz L, et al. (2019) "The preparation and characterization of Co–Ni nanoparticles and the testing of a heterogenized Co–Ni/alumina catalyst for CO hydrogenation." Catalysts 10: 18.

[38] Wang N, Hang T, Chu D, Li M (2015) "Three-dimensional hierarchical nanostructured Cu/Ni–Co coating electrode for hydrogen evolution reaction in alkaline media." Nano-micro letters 7: 347.

[39] Lei Y, Li J, Wang Y, et al. (2014) Rapid microwave-assisted green synthesis of 3D hierarchical flower-shaped NiCo2O4 microsphere for high-performance supercapacitor. ACS applied materials & interfaces 6: 1773.

[40] Marco J, Gancedo J, Gracia M, Gautier J, Ríos E, Berry F (2000) Characterization of the nickel cobaltite, NiCo2O4, prepared by several methods: an XRD, XANES, EXAFS, and XPS study. Journal of Solid State Chemistry 153: 74.

[41] Guan H, Peng B, Gong D, Han B, Zhang N (2021) "Electrochemical Enhanced Detection of Uric Acid Based on Peroxidase-like Activity of Fe3O4@ Au." Electroanalysis 33: 1736.

[42] Hassanvand Z, Jalali F (2019) Simultaneous determination of l-DOPA, l-tyrosine and uric acid by cysteic acid-modified glassy carbon electrode. Materials Science and Engineering: C 98: 496.

[43] Lv J, Li C, Feng S, et al. (2019) "A novel electrochemical sensor for uric acid detection based on PCN/MWCNT." Ionics 25: 4437.

[44] Ma L, Zhang Q, Wu C, Zhang Y, Zeng L (2019) "PtNi bimetallic nanoparticles loaded MoS2 nanosheets: Preparation and electrochemical sensing application for the detection of dopamine and uric acid." Analytica chimica acta 1055: 17.

[45] Tsierkezos NG, Ritter U, Thaha YN, Downing C, Szroeder P, Scharff P (2016) "Multi-walled carbon nanotubes doped with boron as an electrode material for electrochemical studies on dopamine, uric acid, and ascorbic acid." Microchimica Acta 183: 35.

[46] Wang C, Du J, Wang H, et al. (2014) A facile electrochemical sensor based on reduced graphene oxide and Au nanoplates modified glassy carbon electrode for simultaneous detection of ascorbic acid, dopamine and uric acid. Sensors and Actuators B: Chemical 204: 302.

[47] Wu YQ, Chen XY, Ji PT, Zhou QQ (2011) "Sol–gel approach for controllable synthesis and electrochemical properties of NiCo2O4 crystals as electrode materials for application in supercapacitors." Electrochimica Acta 56: 7517.

[48] Kumar A, Furtado VL, Gonçalves JM, et al. (2020) "Amperometric microsensor based on nanoporous gold for ascorbic acid detection in highly acidic biological extracts." Analytica Chimica Acta 1095: 61.

[49] Manjunatha C, Chirag V, Shivaraj BW, Srinivasa N, Ashoka S (2020) "One pot green synthesis of novel rGO@ ZnO nanocomposite and fabrication of electrochemical sensor for ascorbic acid using screen-printed electrode." Journal of Nanostructures 10: 531.

[50] Zou Ce, Zhong J, Li S, et al. (2017) "Fabrication of reduced graphene oxide-bimetallic PdAu nanocomposites for the electrochemical determination of ascorbic acid, dopamine, uric acid and rutin." Journal of Electroanalytical Chemistry 805: 110.

[51] Abellán-Llobregat A, Vidal L, Rodríguez-Amaro R, Canals A, Morallon E (2018) "Evaluation of herringbone carbon nanotubes-modified electrodes for the simultaneous determination of ascorbic acid and uric acid." Electrochimica Acta 285: 284.

[52] Ji D, Liu Z, Liu L, et al. (2018) "Smartphone-based integrated voltammetry system for simultaneous detection of ascorbic acid, dopamine, and uric acid with graphene and gold nanoparticles modified screen-printed electrodes." Biosensors and Bioelectronics 119: 55.

[53] Satheesh Babu T, Varadarajan D, Murugan G, Ramachandran T, Nair BG (2012) Journal of Applied Electrochemistry 42: 427.

[54] Chu Y, Zhou H, Wang X, et al. (2023) A flexible and self-supported nanoporous gold wire electrode with a seamless structure for electrochemical ascorbic acid sensor. Microchemical Journal 186: 108259.

[55] Xi L, Ren D, Luo J, Zhu Y (2010) "Electrochemical analysis of ascorbic acid using copper nanoparticles/polyaniline modified glassy carbon electrode." Journal of electroanalytical chemistry 650: 127.

[56] Ghanbari K, Hajheidari N (2015) "ZnO–CuxO/polypyrrole nanocomposite modified electrode for simultaneous determination of ascorbic acid, dopamine, and uric acid." Analytical Biochemistry 473: 53.

[57] Wang M, Cui M, Liu W, Liu X (2019) Highly dispersed conductive polypyrrole hydrogels as sensitive sensor for simultaneous determination of ascorbic acid, dopamine and uric acid. Journal of Electroanalytical Chemistry 832: 174.

[58] Shao L, Wang X, Yang B, et al. (2017) "A highly sensitive ascorbic acid sensor based on hierarchical polyaniline coated halloysite nanotubes prepared by electrophoretic deposition." Electrochimica Acta 255: 286.

[59] Shen Y, Zheng L (2023) Polyaniline-poly (methylene blue) nano-rod composites as an electrochemical sensor for sensitive determination of ascorbic acid. International Journal of Electrochemical Science 18: 6.

[60] Tukimin N, Abdullah J, Sulaiman Y (2018) Electrodeposition of poly (3, 4-ethylenedioxythiophene)/reduced graphene oxide/manganese dioxide for simultaneous detection of uric acid, dopamine and ascorbic acid. Journal of Electroanalytical Chemistry 820: 74.

[61] Chang AS, Tahira A, Chang F, et al. (2023) "Highly Heterogeneous Morphology of Cobalt Oxide Nanostructures for the Development of Sensitive and Selective Ascorbic Acid Non-Enzymatic Sensor." Biosensors 13: 147.

[62] Habibi B, Pournaghi-Azar MH (2010) "Simultaneous determination of ascorbic acid, dopamine and uric acid by use of a MWCNT modified carbon-ceramic electrode and differential pulse voltammetry." Electrochimica Acta 55: 5492.

[63] Zheng D, Ye J, Zhou L, Zhang Y, Yu C (2009) "Simultaneous determination of dopamine, ascorbic acid and uric acid on ordered mesoporous carbon/Nafion composite film." Journal of Electroanalytical Chemistry 625: 82.

[64] Jo A, Kang M, Cha A, et al. (2014) "Nonenzymatic amperometric sensor for ascorbic acid based on hollow gold/ruthenium nanoshells." Analytica chimica acta 819: 94.

[65] Han D, Han T, Shan C, Ivaska A, Niu L (2010) "Simultaneous determination of ascorbic acid, dopamine and uric acid with chitosan-graphene modified electrode." Electroanalysis 22: 2001.

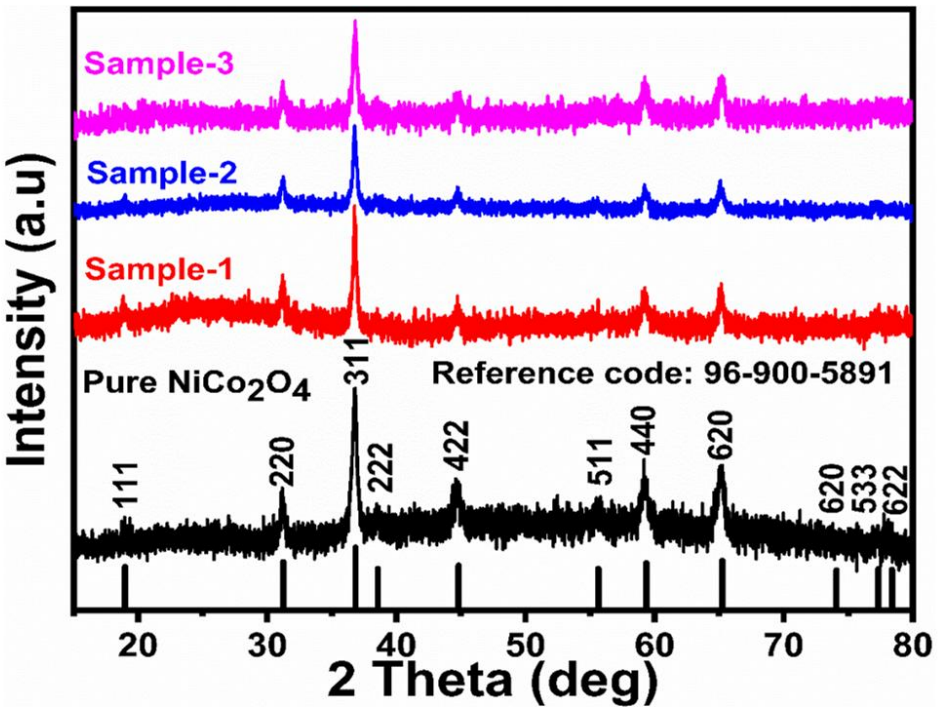

Figure 1: XRD Pattterns of various $NiCo_2O_4$ nanostructures inclduign pristine and preared with 5 mL (Sample 1), 10mL (Sample 2) and 15 mL (Sample 3) of galric leaves extract.

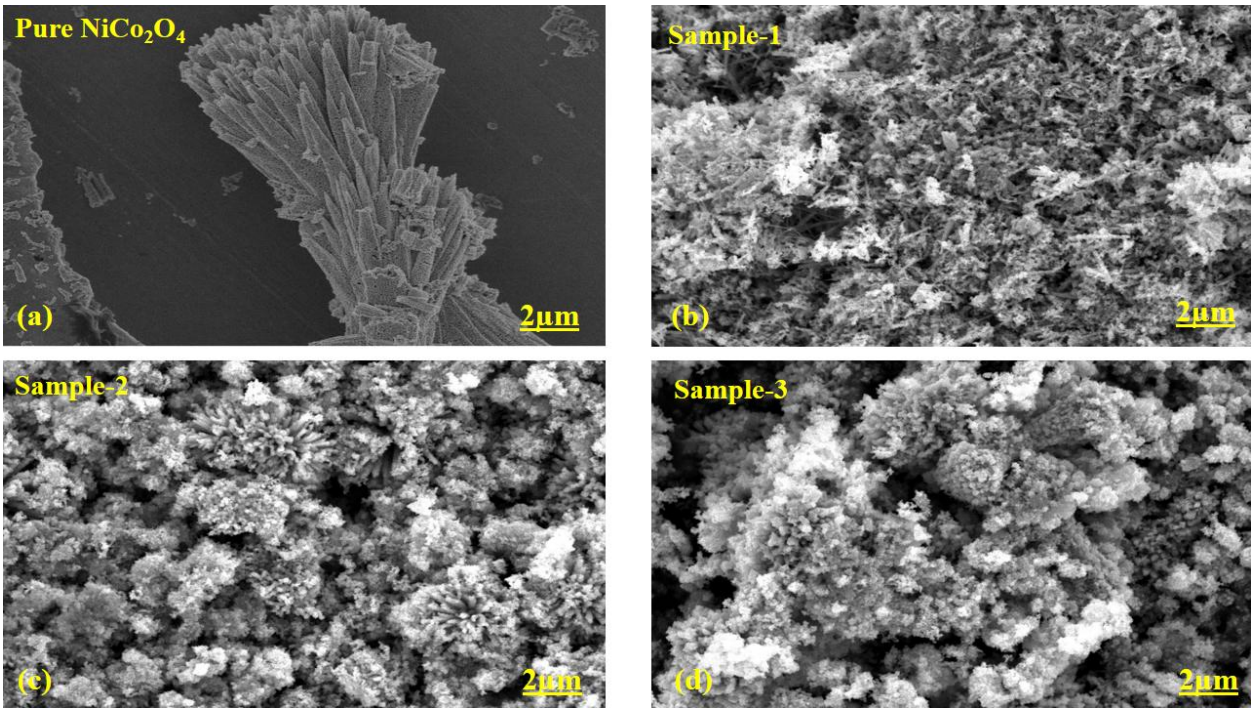

Figure 2: (a-d) SEM iamges of various $NiCo_2O_4$ nanostructures inclduign pristine and preared with 5 mL (Sample 1), 10mL (Sample 2) and 15 mL (Sample 3) of galric leaves extract.

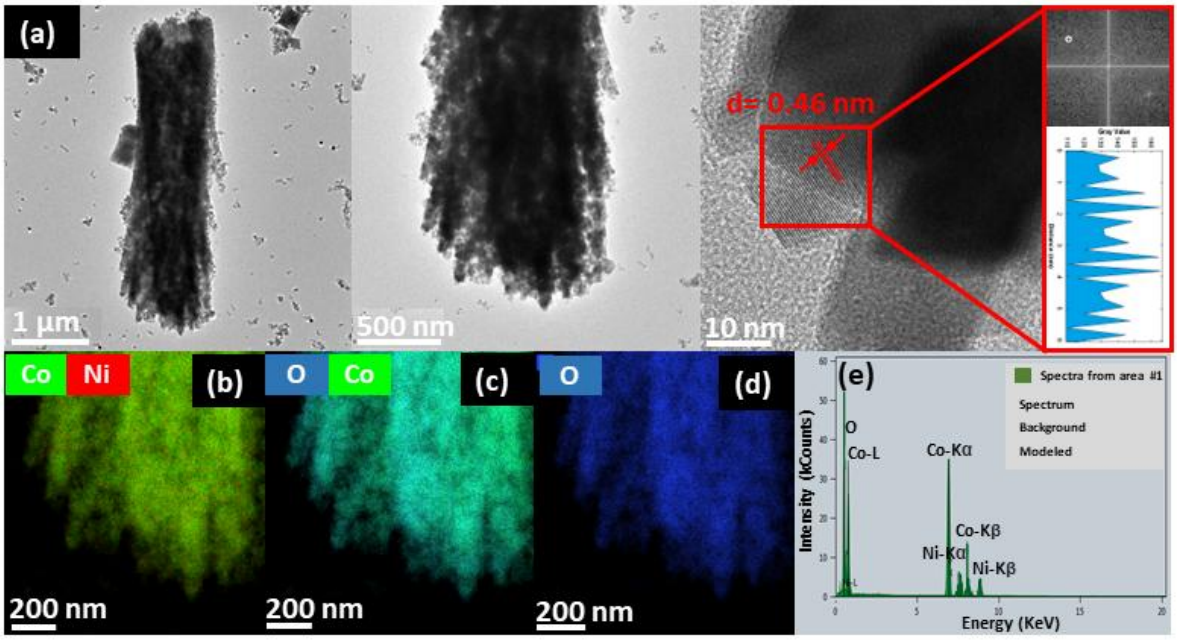

Fig.3: HRTEM analysis of pristine $NiCo_2O_4$ nanostructures (a) HRTEM images and FFT conversion at right side with d-spacing value (b), (c), and (d) corresponding elemental mapping (e) EDS spectra for elemental existence.

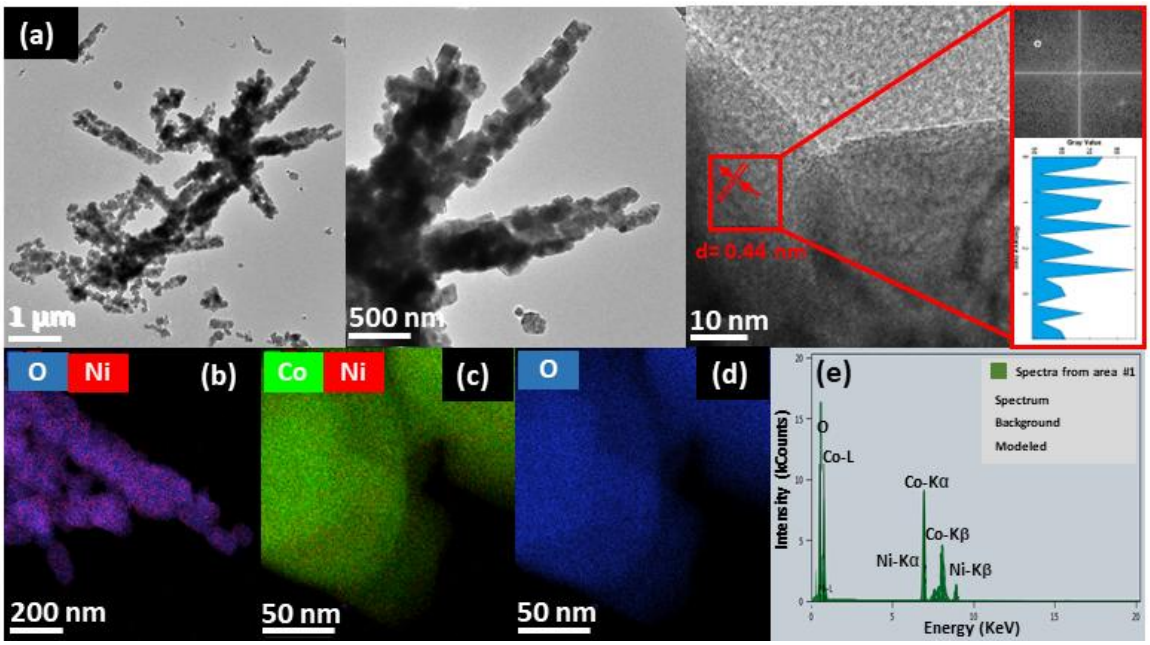

Fig. 4: HRTEM analysis of $NiCo_2O_4$ nanostructures prepared with 10 mL of galric leaves extract (a) HRTEM images and FFT conversion at right side with d-spacing value (b), (c), and (d) corresponding elemental mapping (e) EDS spectra for elemental existence.

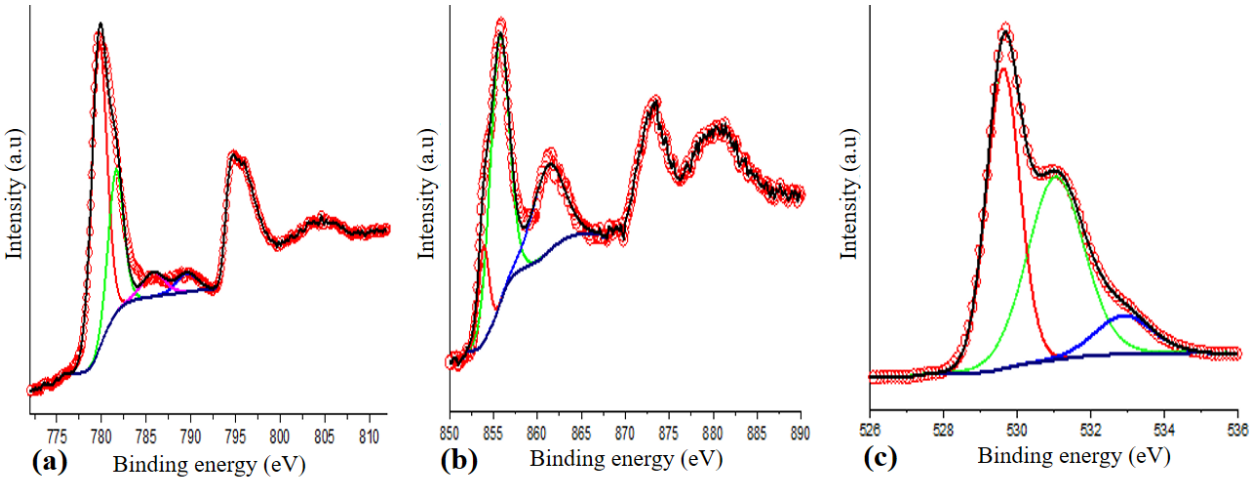

Figure 5: XPS resolved spectra (a) Co 2p, (b) Ni 2p, (c) O 1s of $NiCo_2O_4$ nanostructures prepared with 10 mL of galric leaves extract.

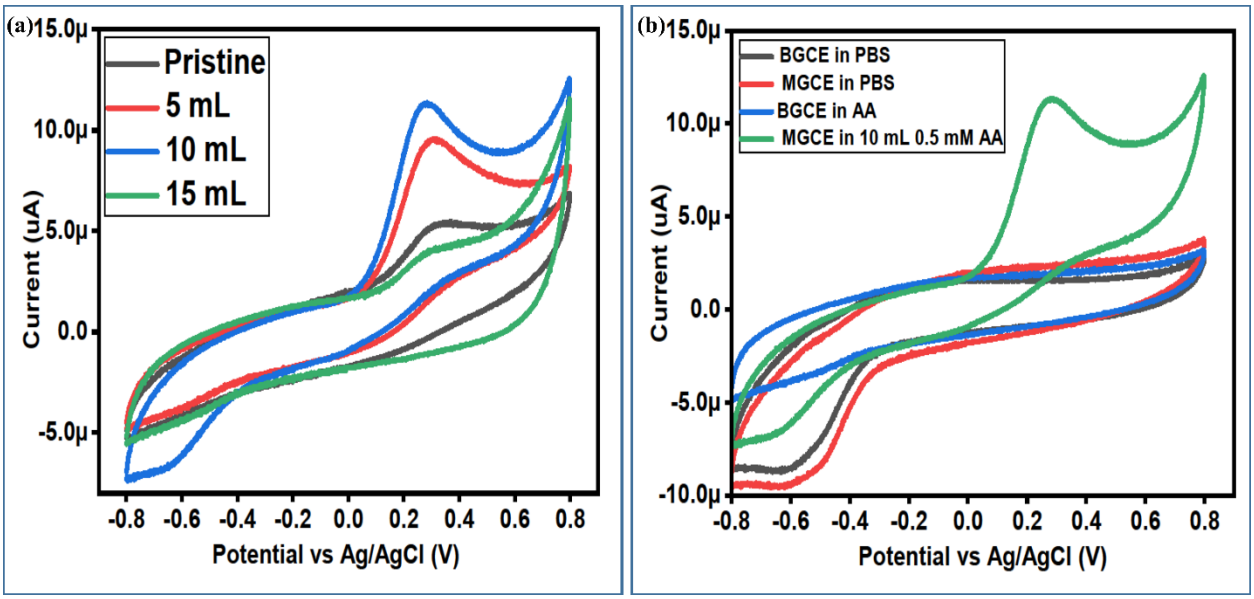

Figure 6. (a) Cyclic voltammograms at a scan rate of 50 mV/s of MGCE with 5 mL, 10 mL and 15 mL garlic leaves extract assistd $NiCo_2O_4$ and pristine $NiCo_2O_4$-modified GCE in the presence of 0.5 mM of AA in 0.1M PBS pH 7.4 **(b)** Cyclic voltammograms at 50 mV/s of bare GCE and modified with 10 mL assisted NiCo2O4 in electrolyte and in the presence of 0.5 mM AA in 0.1M PBS pH 7.4.

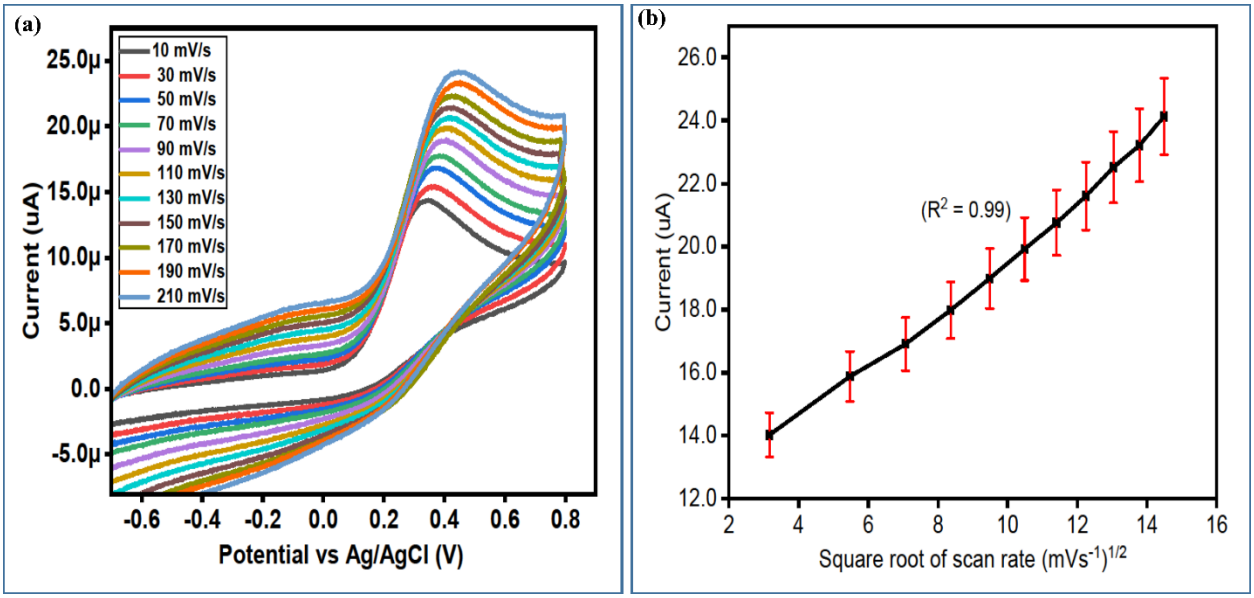

Figure 7. (a) Cyclic voltammograms at a scan rate of 50 mV/s of MGCE with 10 mL garlic leaves extract assisted $NiCo_2O_4$ modified GCE in the presence of 0.5 mM of AA in 0.1M PBS pH 7.4. **(b)** Linear plot of peak current against square root of scan rate.

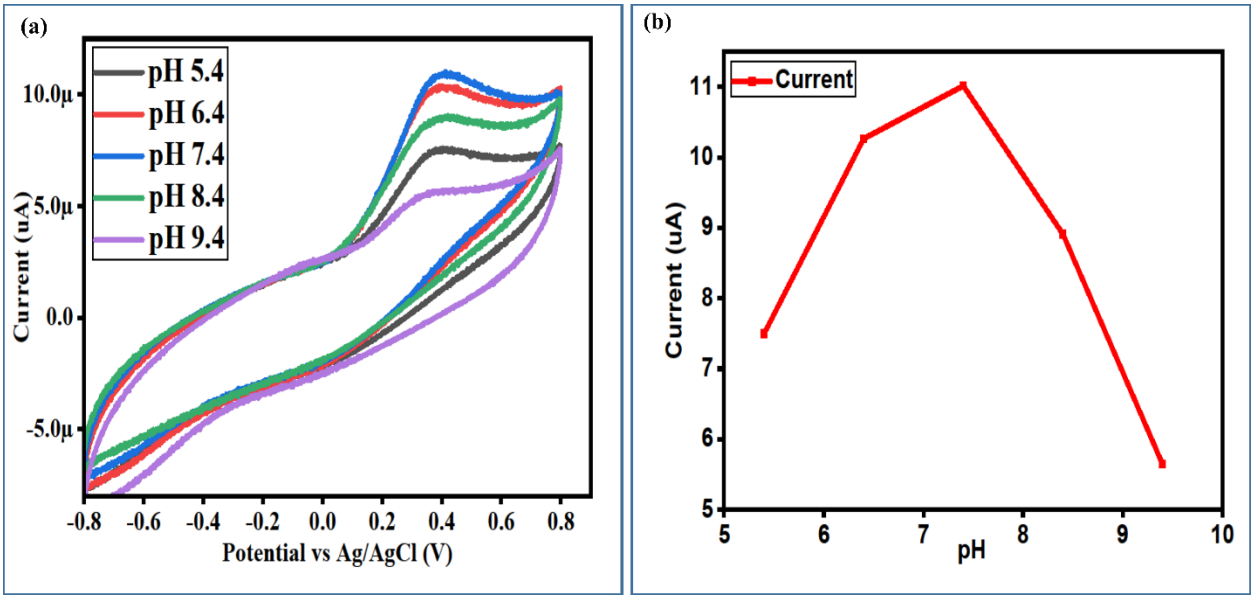

Figure 8. (a) Cyclic voltammograms at a scan rate of 50 mV/s of MGCE with 10 mL of garlic leave extract assisted $NiCo_2O_4$ -modified GCE in the presence of different pH values of 0.5 mM of AA in 0.1M PBS.. **(b)** Linear plot of peak current versus different pH values of 0.5 mM of AA in 0.1M PBS.

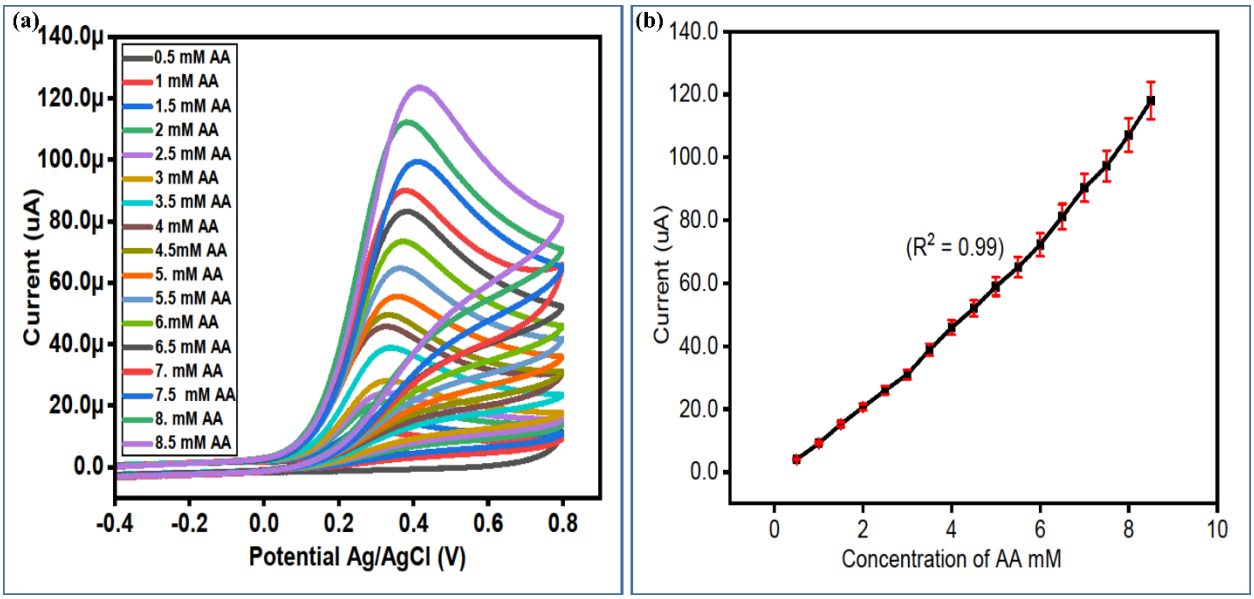

Figure 9. Cyclic voltammograms at a scan rate of 50 mV/s of MGCE with 10 mL of garlic leaves extract assisted $NiCo_2O_4$ in the presence of various concentrations of AA in 0.1M PBS pH 7.4, (b) Linear plot of peak current versus successive increase of AA concentrations.

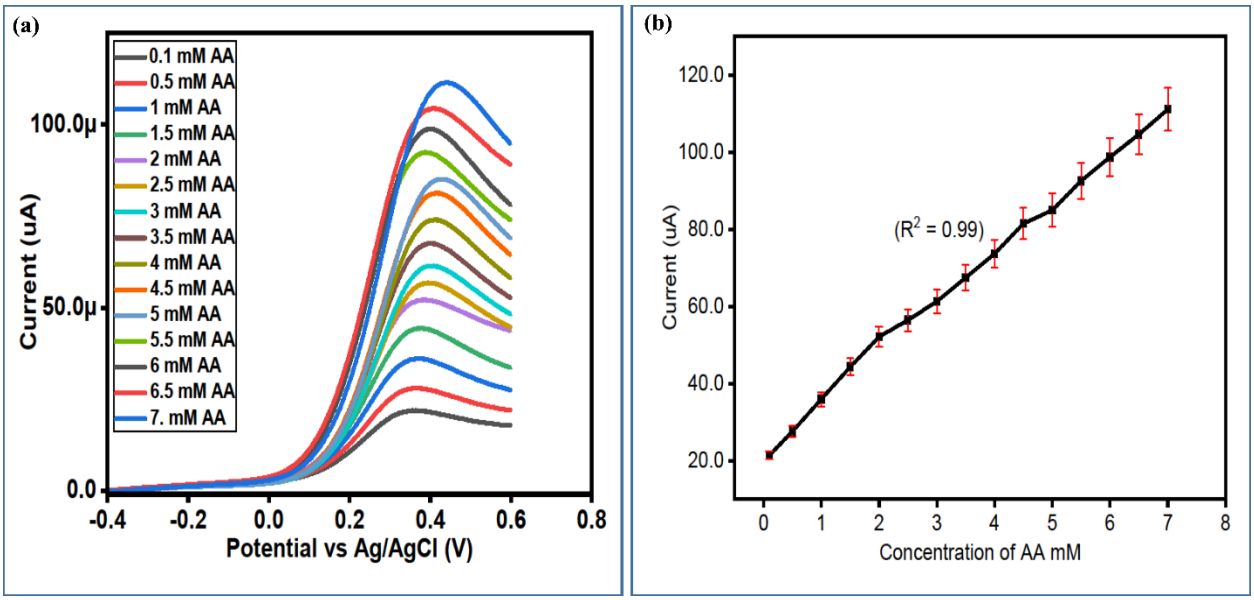

Figure 10. **(a)** Linear sweep voltammetry at a scan rate of 10 mV/s of MGCE with 10 mL of garlic leaves extract assisted $NiCo_2O_4$ in the presence of various concentrations of AA in 0.1M PBS pH 7.4, (b) Linear plot of peak current versus successive increase of AA concentrations.

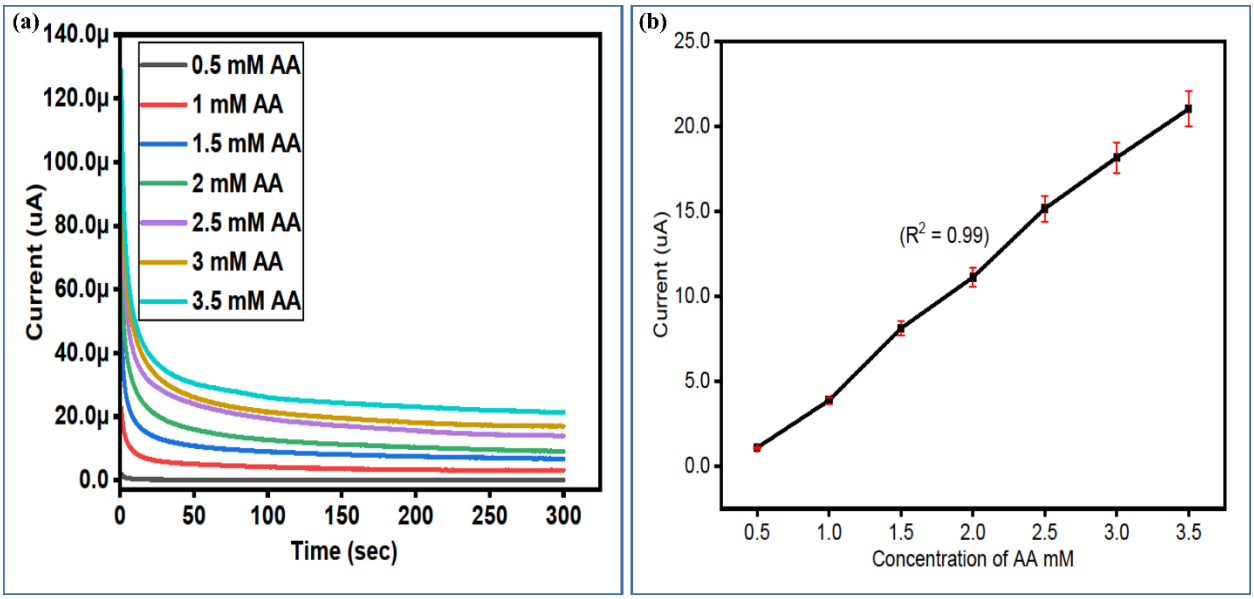

Figure 11. (a) Chronoamperometric response curves measured at an applied potential of 0.3V of MGCE with 10 mL of garlic; eaves extract assisted $NiCo_2O_4$ in the presence of various concentrations of AA in 0.1M PBS pH 7.4, (b) Linear plot of peak current versus successive increase of AA concentrations.

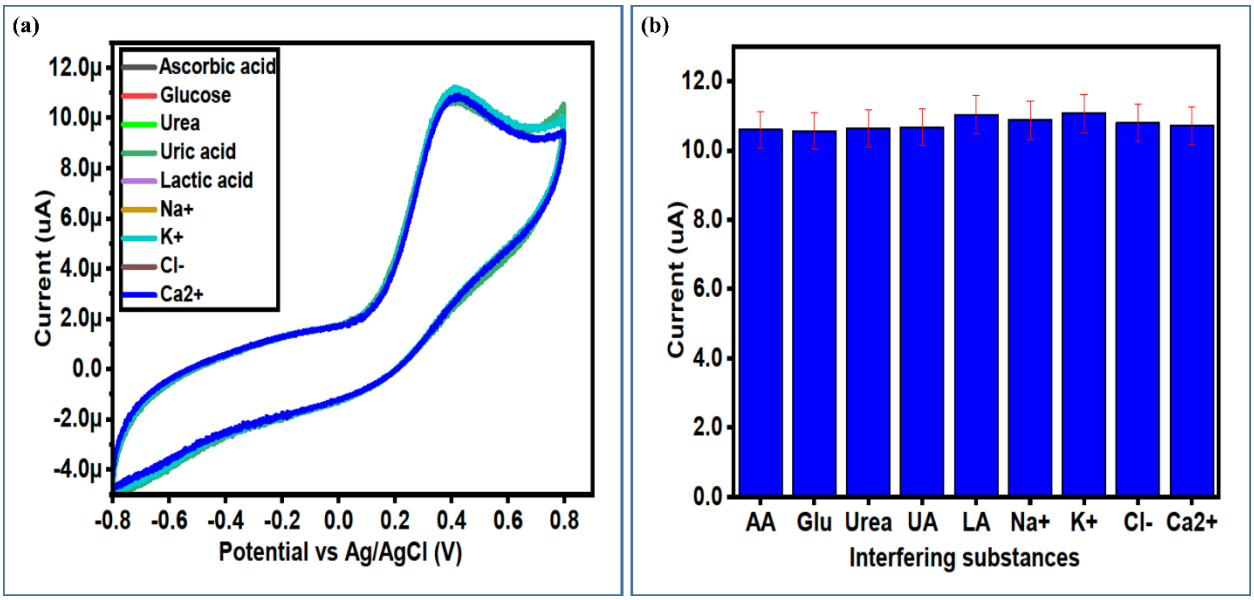

Figure 12 . (a) Cyclic voltammograms at a scan rate of 50 mV/s of MGCE with 10 mL of garlic leaves extract assisted $NiCo_2O_4$ in the presence of 0.5mM AA and other competing interfering

agents (20%) in 0.1M PBS pH 7.4, (b) bar graph of peak current with addition of interfering species for the illustration of variation of peak current.

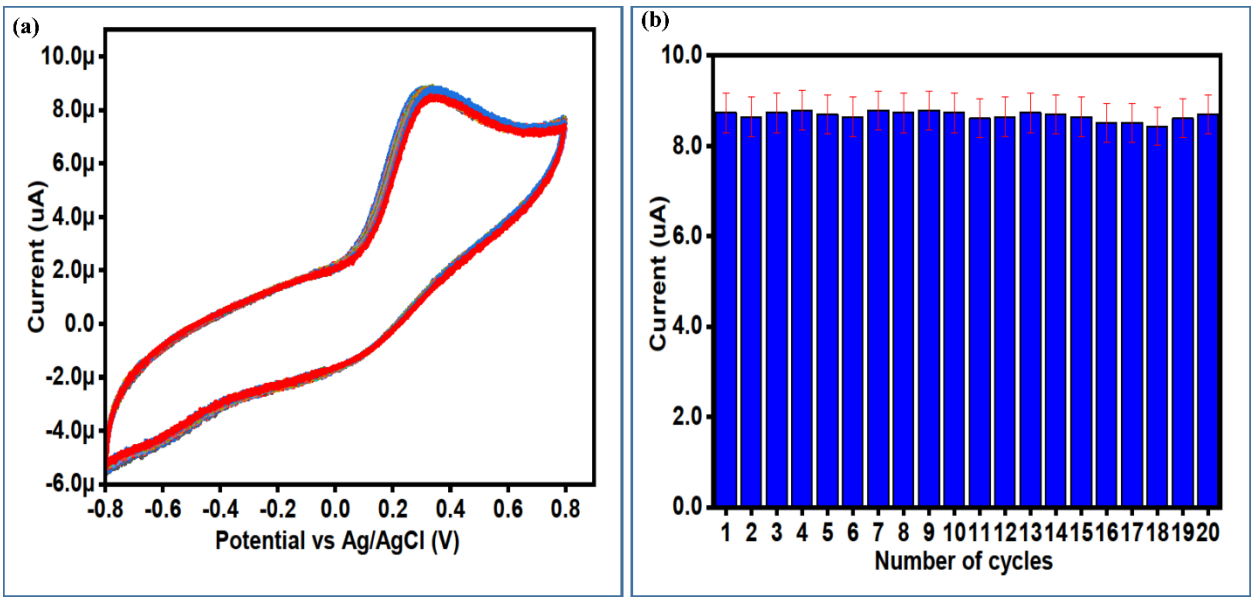

Figure 13. Cyclic voltammograms at a scan rate of 50 mV/s of MGCE with 10 mL of garlic leaves extract assisted $NiCo_2O_4$ in the presence of 0.5mM AA in 0.1M PBS pH 7.4, (b) bar graph of peak current for the description of change in the peak current with increasing number of CV cycles. Linear plot of peak current versus successive increase of AA concentrations.

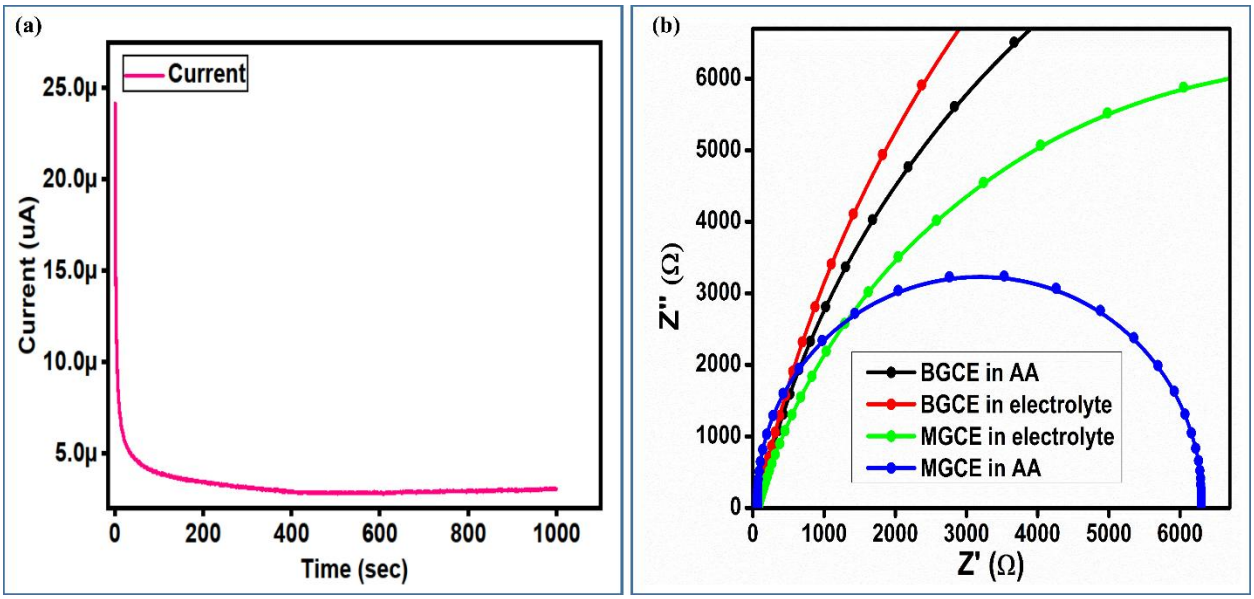

Figure 14. (a) Chronoamperometric response of MGCE with 10 mL of garlic extract assisted $NiCo_2O_4$ in 0.5mM prepared in 0.1M PBS pH 7.4 for the demonstration of stability of modified electrode, **(b)** EIS Nyquist plots collected for the MGCE with and 10 mL of garlic extract assisted $NiCo_2O_4$ in 0.5mM AA using frequency range of 100 kHz to 1 Hz, amplitude of 10 mV and biasing potential of 0.6V.

Table 1: Performance comparison of the enzyme-free sensor based on $NiCo_2O_4$ nanostructures grown with 10 mL garlic leaves extract versus several non-enzymatic AA sensors in the literature.

Sensing electrode Material	**Linear range (µM)**	**Detection of limit (µM)**	**References**

NPG	10-1100	2.0	[48]
GCE/Au@Pd-RGO	0.01-100	0.002	[49]
PdAu/rGO/GCE	12.5-700	12.5	[50]
Au-IDA/hCNT	0-600	20	[51]
Graphene-AuNPA/SPA	20-375	1.04	[52]
AuNP/PPy/TiO_2	1-5000	0.1	[53]
S/NP-Au	0.3-923.3	0.0263	[54]
CuNPs/PANI/GCE	3-3500	2	[55]
ZnO-Cu_x/PPy/GCE	200-1000	25	[56]
PPy/hydrogel/GCE	2.5-1500	1.28	[57]
PANI-HNTs/TTO	5-5500	0.21	[58]
PANI-PMB/CPE	4-110	1.3	[59]
Pd/CNF-CPE	50-4000	15	[59]
RGO/GCE	30-350	14.8	[60]
Co_3O_4/GCE	500-6500	1	[61]
MWCNT/CCE	15-800	7.71	[62]
OMC/Nafion	40-800	20	[63]
Au/Ru nanoshells /GCE	5-2000	2.2	[64]
Chitosan-graphene	50-1200	50	[65]
$NiCo_2O_4$ Nanostructure(Garlic leaves extract)	**500-8500**	**10**	**Present work**

Table 2: Practical performance of $NiCo_2O_4$ prepared with 10 mL of garlic leaves extract using standard addition method by following (%) recovery method

Sample ID	Added (mM)	Found (mM)	(%)Recovery	RSD (%)
Commercial orange juice	0.5	0.523 ± 0.0051	105	0.541
	1	1.494 ± 0.0065	100	0.492
	1.5	3.082 ± 0.0071	103	0.523
Ce-cone tablet	0.5	0.513 ± 0.0082	103	0.513
	1	1.521 ± 0.0048	101	0.484
	1.5	3.062 ± 0.0061	102	0.535